Design and analysis of the separating device for peanut half-feed combined harvesting

Dongjie Li[1,3], Jalin Hou[1*], Dongwei Wang[2,3], Zenghui Gao[3], Zengcun Chang[1,3]

(1. *College of Mechanical and Electronic Engineering, Shandong Agricultural University, Taian, 271000, Shandong, China*;
2. *College of Mechanical and Electrical Engineering, Qingdao Agricultural University, Qingdao 266109, Shandong, China*;
3. *Yellow River Delta Intelligent Agricultural Machinery Equipment Industry Research Institute, Dongying 257100, Shandong, China*)

Abstract: During combined peanut harvesting operations, the separating device plays a crucial role in determining peanuts' damage rate and impurity content. In order to enhance the quality and efficiency of peanut harvesting, this study investigates the separating device of a two-ridge and four-row half-feeder combine harvester. Firstly, the operating principle of the separating device was analyzed, and a combined air-and-screen separating device was selected. Secondly, based on the movement state of peanut pod impurities in different sections of the separating device surface, the theoretical analysis of peanut pod impurity movement was carried out, and the peanut pod impurity dynamics model was constructed. At the same time, CFD software was used to analyze the airflow field inside the separating device. Moreover, the test factors affecting the separating effect were explored: fan wind speed, separating device surface inclination, and vibration frequency. The optimal working parameters of the device were determined as follows: a fan wind speed of 8.9 m/s, a separating device surface inclination angle of 8.3° concerning the horizontal, and a separating device vibration frequency of 7.2 Hz. The impurity content rate of the peanut pods was 1.48%, and the damage rate of the separating device was 1.61%. Finally, the impurity content of peanuts in the validation experiment was 1.53%, and the peanut damage rate was 1.68%. The effectiveness of the separating device operation was verified through field tests. The potential for further research on peanut harvesters is highlighted based on the findings of this study.
Keywords: combine harvester, air-and-screen separating device, peanut, impurity content ratio, damage rate
DOI: 10.25165/j.ijabe.20251801.8711

1　Introduction

In China, the planting area and yield of peanuts have been steadily increasing, according to data from the 2023 China Statistical Yearbook. Within the last five years, peanut yield per unit area has increased yearly, for a total increase of about 200 kg/hm² during this time period. The increasing peanut unit yield further increases the urgent need for mechanization and modernization in the peanut industry.

According to the analysis of peanut planting characteristics in China, peanut harvesting methods can be divided into two-stage harvesting and combined harvesting. At present, most areas use two-stage peanut harvesting[1]. Because the existing combine harvester is poorly adapted to the peanut planting mode in different regions, this study aims to research the characteristics of China's peanut planting mode in relation to peanut combined harvesting machinery[2-4]. However, in the peanut combine harvesting machinery equipment, the separating device has a greater impact on the working effect of the whole machine. There are problems such as high impurity rate

and high damage rate of peanut pods in the machine harvesting process[5,6]. So, peanut-separating device design and testing have been carried out.

The preliminary research found that there are few research methods at home or abroad for scavenging and separation technology that are exclusively geared toward peanut-separating devices. This paragraph summarizes some of the domestic and foreign seed-crop separating methods. The separating methods can be divided into three categories: air-separating, screen-separating, and air-and-screen separating. Xu et al.l.[7] studied the flax threshing and separating device, specifically exploring the airflow separation mechanism for jute materials. They used CFD-DEM coupled simulation technology to determine the separation law of hulled material in the separating system and designed and optimized the flax threshing and separating device. On the other hand, Zhang et al.l.[8] focused on investigating the mechanism of sieve body movement and airflow on the particle group of discharged material during the separating process. The article used the Boltzmann method to analyze the distribution law of the airflow field inside the separating device. Kluge[9] studied the relationship between the motion of material particles and the relative motion of moving sieves. They solved the ejection intensity factor that induces motion between material particles. Zhang[10] examined the working mechanism of a fish scale sieve separating device and analyzed the distribution law of the airflow field inside the separating device. A kinetic model of corn material particles on the fish scale sieve was constructed. The design and optimization of a new type of corn-separating fish scale sieve were described based on the mechanisms of grain penetration and corn shaft clogging of the fish scale sieve. Dai et al.[11-14] investigated the separation of small-seeded crops,

carrying out device design and simulation tests and analyses. Meanwhile, some scholars have conducted impurity separation characteristic analysis based on the characteristics of different crops. Simultaneously, EDEM simulation software was used for numerical simulation analysis, achieving low-loss harvesting and efficient separating effectsts[15-18]. In addition, referring to the harvest patterns of different crops, researchers have analyzed the components and working principles of the whole machine, explored the experimental factors that affect the overall operation of the machine, optimized the coordination relationship between various parameters, and verified the reliability of the machine and device through field experimentsts[19-22].

Through the analyses, the separating principle of the above seed crops has a similar motion principle to peanut separating. Both use air-and-screen separating devices[23,24]. However, the motion model is lacking when the material collides with the device. Therefore, this paper used a two-row, four-row, half-fed peanut combine harvester as the research object. The focus was on exploring the collision motion between materials and devices. The interaction models between pods, impurities, and devices were obtained. In addition, the conditions of pods and impurity motion during air-and-screen separating were further elaborated. The distribution law of the airflow field inside the separating screen was investigated. The design of the separating device was also carried out. The separating device was created, and its operating parameters were optimized. This study provides a reference for optimizing the theory and technology system of the half-feed peanut combine harvesting separating systems in China.

2   Methods and materials

2.1   Structure and working process of the harvester

Figure 1 depicts a peanut combine harvester with two ridges and four rows. The machine mainly comprises a walking device, air-and-screen separating device, L-shaped conveyor, clamping and conveying device, peanut collection device, peanut-picking device, driver's cab, clamping homing device, excavation device, and seedling support device. The machine's workflow mainly employs excavation to unearth peanut pods from the soil. The clamping homing device conveys the peanut plants to the pod-picking device, facilitating the collection of peanut pods. The air-and-screen separating device separates the peanut pods from any impurities in the picking material. After separation, the separated peanut pods undergo another screening process via the L-shaped conveyor chain. At the same time, the peanut pods are guided by the conveyor chain into the peanut collection device, completing the peanut harvesting process.
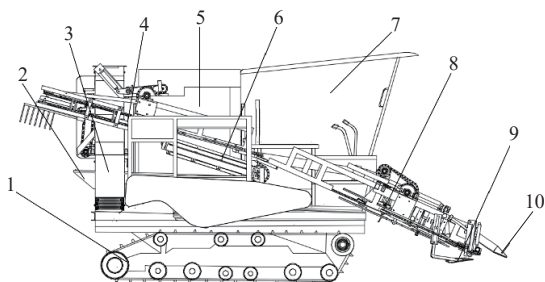
1.Walking device 2. Air-and-screen separating device 3. L-shaped conveyor 4. Clamping and conveying device 5. Peanut collection device 6. Peanut-picking device 7. Driver's cab 8. Clamping homing device 9. Excavation device 10. Seedling support device

Figure 1   Structure of the peanut combine harvester

Figure 2 shows the working process of the air-and-screen separating device. This device separates the sieve frame, surface, eccentric wheel drive mechanism, blower, and seedling discharge device components. The working principle is as follows: the material falls onto the separating sieve surface from top to bottom, and the motor transmits power to the separating sieve surface through the eccentric wheel, resulting in a simple harmonic reciprocating motion of the separating device. Additionally, the device is equipped with a fan that utilizes the difference in the floating characteristics of the material for air-blowing separating. The material can be directed toward the seedling discharge device by adjusting the fan wind speed, screen surface inclination, and vibration frequency appropriately. The peanut pods fall through the gap of the seedling discharge device into the next working section. Impurities such as broken leaves, short stalks, soil, and fruit stalks fall through the gaps on the sieve surface. Long stalks, residual plastic film, and other impurities are blown out of the sieve surface along with the peanut pods as they move toward the seedling discharge device, effectively completing the separating process.
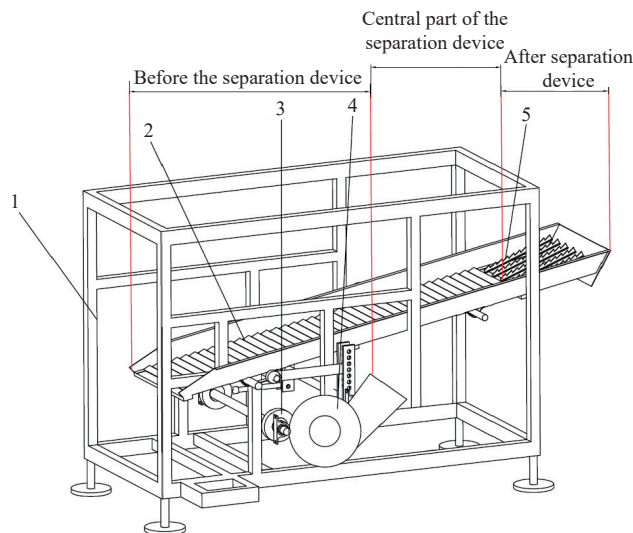
1. Separating sieve frame 2. Separating sieve surface 3. Eccentric wheel drive mechanism 4. Blower 5. Seedling discharge device

Figure 2   Schematic diagram of air-and-screen separating device

2.2   Material screening motion analysis

The working principle of the separating device mainly involves using the motor to drive the eccentric wheel, which provides power for the separating sieve surface. The eccentric wheel pushes the connecting rod CD, causing the separating sieve surface to move along the Y direction. In conjunction with the AB rod, it propels the separating sieve surface forward with impact, effectively separating the peanut and impurity mixture on the sieve surface. Figure 3 illustrates the movement of the screening process, characterized by reciprocating simple harmonic motion.

The motion expression of the separating device is as follows:

Displacement:

$$y = -R\cos\omega t \tag{1}$$

Velocity:

$$V_y = R\omega\sin\omega t \tag{2}$$

Acceleration:

$$a_y = R\omega^2\cos\omega t \tag{3}$$

where, y is the vibrating screen surface displacement, mm; R is the

radius of the eccentric wheel, mm; ω is the angular velocity of the eccentric wheel, rad/s; t is the vibration time of the separating screen, s.
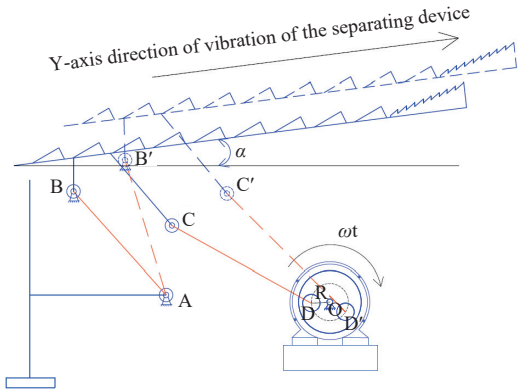
Figure 3   Schematic diagram of the screening motion

By analyzing the principle of motion of the separating device, it can be observed that when the separating sieve surface tends to move or moves to the right, the acceleration of the separating sieve surface is positive. Therefore, the time range is:

$$\left[0, \frac{\pi}{2\omega}\right] \left[\frac{3\pi}{2\omega}, 2\pi\right] \tag{4}$$
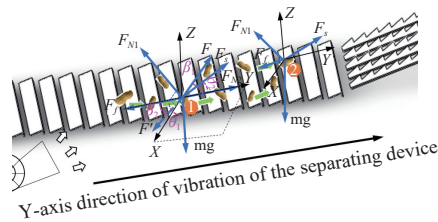
The acceleration of the separating sieve surface is negative when the separating sieve surface tends to move to the left. The time range for this occurrence is:

$$\left[\frac{\pi}{2\omega}, \frac{3\pi}{2\omega}\right] \tag{5}$$

2.3   Material screening motion analysis

When the time interval is $\left[0, \frac{\pi}{2\omega}\right]$ $\left[\frac{3\pi}{2\omega}, 2\pi\right]$, the acceleration direction of the separation device is positive, and the inertial force direction is along the positive Y-axis. When the time interval is $\left[\frac{\pi}{2\omega}, \frac{3\pi}{2\omega}\right]$, the acceleration direction of the separating device is negative, and the inertial force direction is negative along the Y-axis. When the material contacts the separating sieve surface, its movement speed along the Y direction surpasses the surface's. The direction of the green arrow in the picture is the direction of material movement. YOZ plane is the vertical plane of the separator surface. XOY plane is the parallel plane of the separator surface, i.e., the inclined side of the separator surface. Consequently, the material moves towards the right along the separating sieve surface. Due to the ladder shape of the sieve surface, the peanut force state is divided into two cases. The first is when the peanut is on the vertical side of the stepped separating sieve surface, as shown in Figure ① below. The second case is when the peanut is on the inclined side of the ladder separating the sieve surface, as shown in Figure ② below. The forces at different positions are shown in Figure 4.
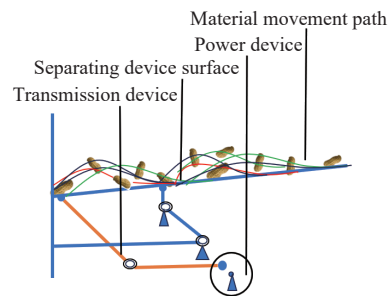
a. Force analysis diagram   b. Schematic diagram of movement patterns

Figure 4   Schematic diagram of material moving to the right

As shown in Figure 4, the inertial force F exerted by the material on the sieve surface is:

$$F = -\omega^2 mA \sin \omega t \tag{6}$$

The friction force F_f is:

$$F_f = \mu F_{N1} = F_{N1} \tan\varphi \tag{7}$$

The expression for wind power F_s of the wind turbine is:

$$F_s = k\rho S v^2 \tag{8}$$

where, m is the mass of the material, g; A is the amplitude of the separation sieve surface, mm; k is the floating coefficient; F_{N1} is the support force, N; φ is the friction angle, (°); ρ is the density of air, 1.29 kg/m³; S is the area of the material facing the wind, m²; v is the airflow velocity of the fan, m/s.

When the material slides upwards, the direction of friction is opposite to that of the material's sliding direction. Wind, inertia, and friction contribute to the upward acceleration of the material. When the direction of acceleration of the separating sieve surface is positive, the motion model of the material is:

$$mg\cos\theta_1 + F_f < F_s\cos\theta_2 + F\cos\beta_1 + F_{N2} \tag{9}$$

where, F_{N2} is the collision force between the vertical side of the step and the peanut. When the peanut moves in the positive Y-axis direction, $F_{N2} > 0$. The simplification of Equation (9) yields:

$$F_{N1} < k\rho sv^2\cos\theta_2 - mA\omega^2\sin\omega t\cos\beta_1 - mg\cos\theta_1 + F_{N2} \tag{10}$$

Similarly, when the direction of acceleration of the separating sieve surface is negative, the motion model of the material sliding upwards is:

$$F_{N1} < k\rho sv^2\cos\theta_2 + mA\omega^2\sin\omega t\cos\beta_2 - mg\cos\theta_1 + F_{N2} \tag{11}$$

Through the analysis of the material's upward sliding model, several critical conditions can be observed. When the acceleration is positive, there is a positive correlation between the upward sliding movement of the material and the wind power of the fan, vibration frequency, and vibration amplitude. Conversely, when the acceleration is negative, the upward sliding motion of the material is negatively correlated with the wind power of the fan but positively correlated with the vibration frequency and vibration amplitude.

When the material slides down to the left along the separating sieve surface, the separating sieve material force model is shown in Figure 5. When the direction of acceleration of the separating sieve is positive, the motion model of the material particles is:

a. Force analysis diagram　　　　　　　b. Schematic diagram of movement patterns
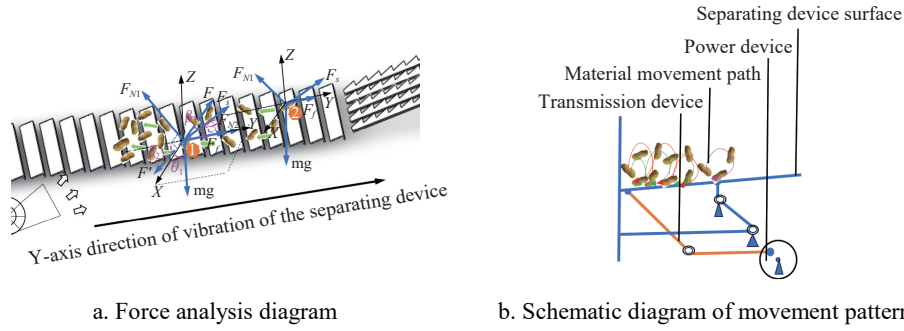
Figure 5　Schematic diagram of material moving to the left

$$mg\cos\theta_1 > F_f + F_S\cos\theta_2 + F\cos\beta_1 \tag{12}$$

The simplification of Equation (12) yields：

$$F_{N1} < mg\cos\theta_1 - k\rho sv^2\cos\theta_2 + mA\omega^2\sin\omega t\cos\beta_1 \tag{13}$$

Similarly, when the direction of acceleration of the separating sieve is negative, the motion model of the material sliding down is:

$$F_{N1} < mg\cos\theta_1 - mA\omega^2\sin\omega t\cos\beta_2 - k\rho sv^2\cos\theta_2 \tag{14}$$

From the material sliding motion model, critical conditions can be determined. When the direction of acceleration on the separating sieve surface is positive, there is a positive correlation between material sliding motion and both vibration frequency and amplitude. On the other hand, material sliding motion and wind force have a negative correlation. When the direction of acceleration on the

separating sieve surface is negative, there is a negative correlation between material sliding motion and vibration frequency, amplitude, and wind force.

As shown in Figure 6, when the material is thrown off the separating sieve surface, the support force and friction become zero. The acceleration along the horizontal and vertical directions of the separating sieve surface are:

$$\begin{cases} a_y = k\rho S v^2\cos\theta + mA\omega^2\sin(\omega t)\cos\beta - g\sin\gamma \\ a_z = k\rho S v^2\cos\theta + mA\omega^2\sin(\omega t)\cos\beta - g\sin\gamma \end{cases} \tag{15}$$

where, θ is the angle between the direction of the wind force and the separating sieve surface, (°); γ is the angle of inclination of the separating sieve surface, (°); β is the angle of the direction of the inertia force of the separating sieve surface, (°).

a. Force analysis diagram　　　　　　　b. Schematic diagram of movement patterns
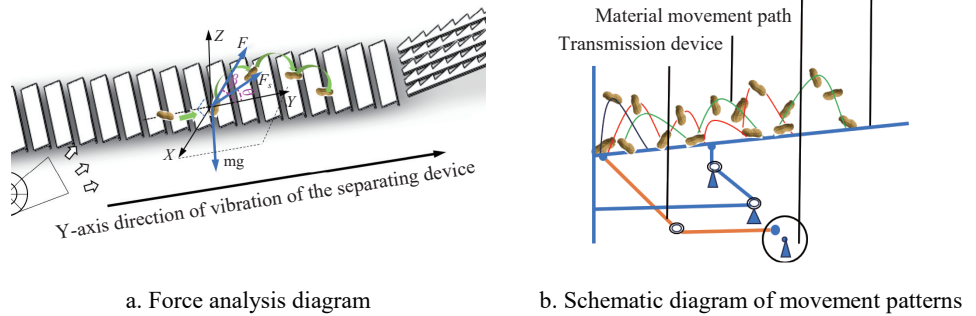
Figure 6　Schematic diagram of the material "thrown up and bounced"

When the material is thrown up and bouncing, the separation screen's movement is analyzed by analyzing the relationship between the movement of the separating screen and factors such as vibration frequency, vibration amplitude, fan wind speed, and screen surface inclination.

2.4　Test equipment and materials

The middle and back sections of the separating screen are mainly air-separating. An anemometer (model Huashengchang DT-8880, wind speed range 0.2-20 m/s, measurement accuracy ±5%) was used to measure the airflow velocity inside the peanut harvester separating device. Refer to GB/T 1236-2000 Test Methods for Aerodynamic Performance of Ventilators for testing standards. The air velocity was measured at multiple points above and below the separating sieve to determine the working parameter range of the fan speed. Fluent software was used to simulate the airflow field. The effect of fan speed on airflow velocity was analyzed in order to provide the basis for carrying out field tests at a later stage.

In order to evaluate the actual operational effect of the device, a field experiment was conducted on October 2, 2022, at the peanut

plantation in Pingdu City, Shandong Province, China (119°97′E, 36°77′N), as shown in Figure 7. The experimental setup included a two-row, four-ridge combined peanut harvester, a speed controller, a vernier caliper, an electronic scale, and other auxiliary tools such as a measuring tape, stainless steel ruler, and sample bags. The selected peanut variety for the experiment was "Yuhua No.14" at its mature stage[25,26].

The test was carried out during the machine's operation. Random samples were taken three times at the pod outlet of the separating device. The sample taken each time was 3 kg at maximum. The sample from the pod outlet was mixed well, and a small sample of 500 g was taken. Complete peanut pods (without removing the stalks on the peanut pods), broken peanut pods, and impurities were sorted out, and the impurity content and brokenness indices of the prototype machine were calculated.

In addition, the original damage rate of peanuts must be investigated before the test. A tarpaulin was spread above the separating sieve. Three random samples were taken at the tarpaulin, each with a peanut pod mass of not less than 200 g. Broken and

intact peanut pods were sorted, their total mass was weighed separately, and the average value was calculated.

Figure 7   Field experiment

Original damage rate:

$$Z_{yp} = \frac{W_p}{W_z} \times 100\% \tag{16}$$

where, Z_{yp} is the original damage rate, %; W_p is the mass of broken pods, g; W_z is the total pods mass, g.

Impurity content ratio:

$$Z_Z = \frac{W_{xz}}{W_{xh}} \times 100\% \tag{17}$$

where, Zz is the impurity content, %; W_{xz} is the mass of impurities in the selected small sample, g; W_{xh} is the mass of the selected sample, g.

Damage rate:

$$Z_p = \frac{W_p}{W_{xh} - W_{xz}} \times 100\% - Z_{yp} \tag{18}$$

where, Z_p is the damage rate, %; W_p is the mass of damaged peanut pods in the small sample, g; Z_{yp} is the original damage rate, %.

3   Results and discussion

3.1   Analyses of the airflow field of the material sorting

Firstly, the structure and parameters of the separating sieve of the half-feed peanut harvester were based on those of the harvester itself. Secondly, a three-dimensional model of the machine was constructed to simplify the simulation process. The simplified model of the separating device only included the sieve body, eccentric mechanism, and fan part, which were then imported into Workbench ICEM for meshing[27]. The meshed model was imported into the software and a simulation of the airflow field was conducted. The fan's wind speed at the initial inlet was set at 10 m/s, and the simulation was run for 1400 iterations. The residual values of the variables in the simulation process were less than 1×10^{-3}, demonstrating convergence. The results of the calculations tended to stabilize with the iteration, which was in line with the convergence conditions.

As shown in the airflow field distribution cloud in Figure 8, the fan outlet's red area indicates the airflow concentration. The sequential stratification of the color represents the gradual dispersion of the airflow. Moreover, the airflow intensity gradually weakened. As shown in the vector diagram of airflow field distribution in Figure 9, the airflow generated by the fan is concentrated in the middle and back end of the separating device. The stratification of the color spread reflects the airflow intensity

from a strong to a weak process. At the same time, due to the obstruction of the sieve body, part of the airflow forms a gyratory state. The gyratory airflow's intensity is gradually weakening, and it does not cause the impurities to fall back.
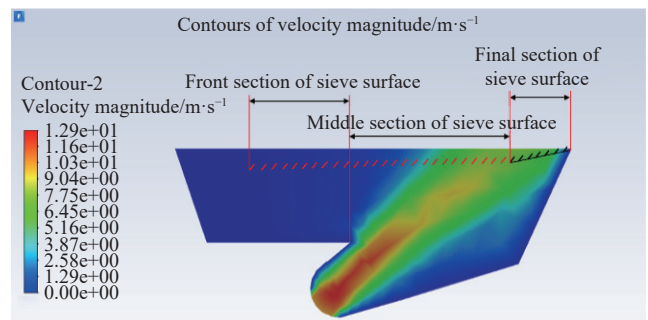
Figure 8   Cloud map of airflow velocity distribution
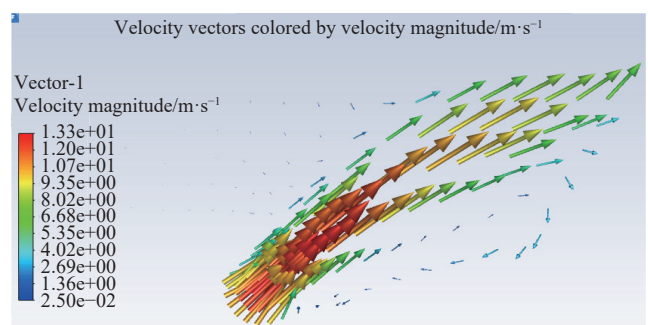
Figure 9   Vector diagram of airflow field distribution

According to the analysis of material components and floating speed, 4%-7% of impurities from short stalks and pod stalks mainly pass through the front section of the sieve during screening, 10%-30% of soil impurities are mainly screened through the front and middle sections of the sieve, and 7%-10% of seedling membranes and long stalks are mainly blown out from the end section of the sieve at the seedling discharge device by using wind power. Since the floating speed of long stalks is 7.1-9.6 m/s, the wind speed at the back section of the sieve is more than 7 m/s and less than 10 m/s. The floating speed of short stalks is 3.1-6.8 m/s, the floating speed of pod stalks is 2.8-6.7 m/s, and the floating speed of branches and leaves of peanut vines is 1.1-3.8 m/s. This impurity is mainly screened by vibration. Considering the floating speed of peanut pods ranging from 11.4-15.5 m/s, it is essential to control the wind speed at any point of the separating sieve surface to be lower than 11 m/s. It is necessary to prevent the airflow speed from being too fast, which will cause the loss of peanut pods. The airflow in the seedling discharge device section is gathered, facilitating the discharge of impurities.

The wind speed on the sieve surface significantly influences the separating efficiency. A higher fan speed leads to increased wind speed on the sieve surface, resulting in improved separating efficiency and a higher loss rate of peanut pods. To examine the effect of fan speed on the airflow on the sieve surface, this study conducted simulations and analyses using fan speeds of 1200 r/min, 1300 r/min, and 1400 r/min, as shown in Figures 10 and 11.

By exploring the distribution law of the airflow field inside the separation sieve, the airflow velocity distribution in the upper and lower part of the separation sieve surface was analyzed. The influence law of different fan speeds on the airflow velocity was obtained, as shown in Figure 12.
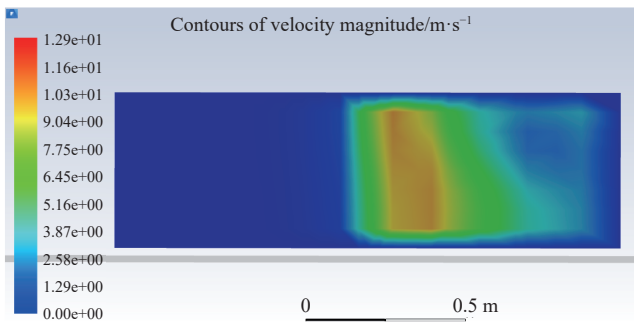
Figure 10　Contours of velocity magnitude below the sieve surface
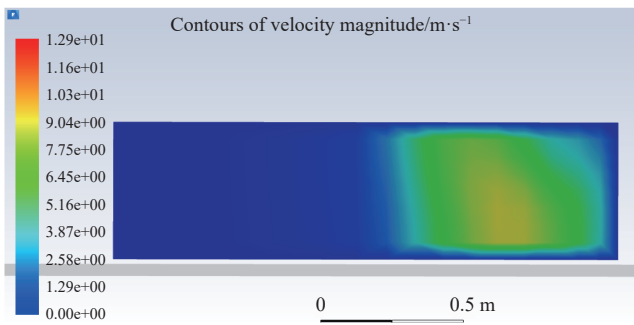
Figure 11　Contours of velocity magnitude above the sieve surface
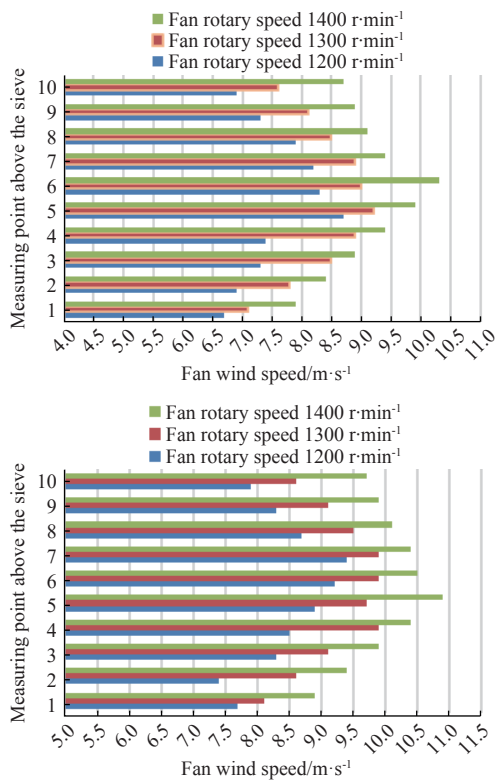
Figure 12　Distribution relationship between fan and
internal airflow

When the fan speed is the same, the airflow velocity underneath the separating screen is significantly higher than above. The airflow velocity increases with the increase in fan speed. When the fan speeds are 1200 r/min, 1300 r/min, and 1400 r/min, respectively, the airflow velocity beneath the separating screen concentrates in the range of 8-11 m/s, while the airflow velocity above the separating screen concentrates in the range of 7 m/s to 10 m/s.

3.2　Field regression experimental design

The results of analyzing the material dynamics model and the airflow field of the separating sieve surface show that the operating

quality of the separating sieve surface is affected by the wind speed of the centrifugal fan, the inclination angle of the screen surface installation, and vibration frequency. To further obtain the optimal parameters for the separating device, three-factor and three-level Box-Behnken center combination tests were conducted on the fan wind speed, screen surface inclination, and vibration frequency using Design Expert software[28]. The test factors and levels are presented in Table 1, while the test program and results are listed in Table 2.

Table 1　Levels of test factors

Code	Experimental factors		
	Fan wind speed X_1/(m·s⁻¹)	Screen surface inclination X_2/(°)	Vibration frequency X_3/(Hz)
−1	8	5	6
0	9	7	7
1	10	9	8

Table 2　Test protocol and response values

Serial number	Experimental factors			Z_Z/%	Z_P/%
	X_1	X_2	X_3		
1	10	7	8	2.48	1.79
2	10	7	6	1.88	2.23
3	9	5	8	2.63	1.96
4	9	7	7	1.62	1.65
5	9	7	7	1.52	1.74
6	8	7	6	2.74	1.45
7	9	9	6	2.02	1.82
8	8	5	7	2.38	1.83
9	8	7	8	2.41	1.69
10	9	5	6	2.42	2.01
11	9	7	7	1.61	1.73
12	9	9	8	1.96	1.58
13	10	9	7	1.48	1.75
14	10	5	7	1.77	2.46
15	9	7	7	1.52	1.63
16	9	7	7	1.53	1.62
17	8	9	7	1.82	1.76

Multiple regression fitting analyses were carried out on the data in Table 2 using Design-Expert software. The ANOVA is listed in Table 3.

Table 3　Detailed Analysis of Variance

Source	Impurity content ratio Z_Z/%			
	Sum of squares	Degree of freedom	F	p
Model	2.99	9	10.45	<0.0001
x_1	0.38	1	124.67	<0.0001
x_2	0.46	1	151.79	<0.0001
x_3	0.022	1	7.26	0.0309
x_1x_2	0.018	1	6.00	0.0441
x_1x_3	0.22	1	71.23	<0.0001
x_2x_3	0.018	1	6.00	0.0441
x_1^2	0.19	1	61.90	0.0001
x_2^2	0.035	1	11.55	0.0115
x_3^2	1.55	1	509.78	<0.0001
Residual	0.021	7		
Lack of fit	0.011	3	1.44	0.3550
Pure error	0.010	4		
All items	3.01	16		

Note: $p<0.01$（**highly significant）; $p<0.05$（*significant）

According to Tables 3 and 4, the overall model is highly significant ($p<0.01$). The lack-of-fit term is not significant ($p>0.05$). The analysis of variance requirements is satisfied. The fan speed (A), screen inclination angle (B), the interaction between fan speed and frequency (AC), the quadratic term of fan speed (A^2), and the quadratic term of frequency (C^2) have a highly significant impact on impurity rate (Z_Z) ($p<0.01$). Frequency (C), the interaction between fan speed and screen inclination angle (AB), the interaction between screen inclination angle and frequency (BC), and the quadratic term of screen inclination angle (B^2) have a significant impact on impurity rate (Z_Z) ($p<0.05$). Fan speed (A), screen inclination angle (B), the interaction between fan speed and screen inclination angle (AB), the interaction between fan speed and frequency (AC), the quadratic term of fan speed (A^2), and the quadratic term of screen inclination angle (B^2) have a highly significant impact on fruit damage rate (Z_P) ($p<0.01$). Frequency (C) has a significant impact on damage rate (Z_P) ($p<0.05$). Other experimental factors do not have a significant impact on the damage rate.

Table 4   Detailed Analysis of Variance

Source	Damage ratio Z_P/%			
	Sum of squares	Degree of freedom	F	p
Model	0.94	9	26.28	0.0001
x_1	0.28	1	70.58	<0.0001
x_2	0.23	1	57.17	0.0001
x_3	0.030	1	7.53	0.0287
x_1x_2	0.10	1	25.70	0.0014
x_1x_3	0.12	1	29.01	0.0010
x_2x_3	9.025E-003	1	2.26	0.1761
x_1^2	0.053	1	13.19	0.0084
x_2^2	0.11	1	28.50	0.0011
x_3^2	7.605E-005	1	0.019	0.8940
Residual	0.028	7		
Lack of fit	0.015	3	1.61	0.3334
Pure error	0.013	4		
All items	0.97	16		

Note: $p<0.01$ (**highly significant); $p<0.05$ (*significant)

As shown in Figure 13，because the points in the normal residual plot for the impurity rate converge to a straight line, the results of the orthogonal experiment for the peanut harvest field trial are reliable.
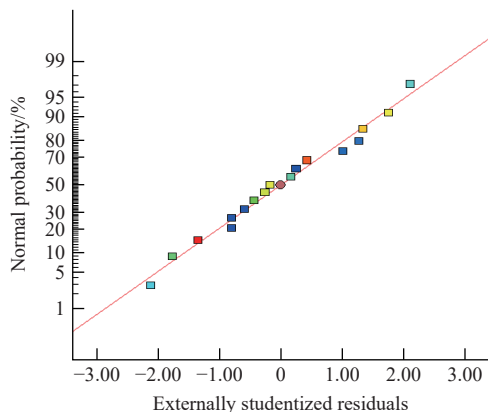
Figure 13   Impurity content ratio residuals normality plot

Because the points in the normal residual plot for the impurity rate converge to a straight line, the results of the orthogonal experiment for the peanut harvest field trial are reliable. The

assumption of normality of errors is reasonable. By comparing the F values, the order of the impact of each factor on pod damage rate is: $C^2>B>A>AC>A^2>B^2>C>AB=BC$. The regression equation for the impurity rate of the peanut-separating device is obtained:

$$Z_Z =1.56 - 0.22A - 0.24B + 0.052C + 0.067AB + 0.23AC - $$
$$0.067BC + 0.21A^2 + 0.091B^2 + 0.61C^2 \qquad (19)$$

From Equation (19), it can be seen that the impurity rate is linearly negatively correlated with fan speed (A) and screen inclination angle (B) and linearly positively correlated with frequency (C). At the same time, it has a quadratic relationship with fan speed (A), screen inclination angle (B), and frequency (C). This indicates that an optimal combination of the three factors exists to minimize the impurity rate of pods.

As shown in Figure 14, because the points in the normal residual plot for damage rate converge to a straight line, the results of the orthogonal experiment for the peanut harvest field trial are reliable. The assumption of normality of errors is reasonable. By ignoring non-significant factors and comparing the F values, the order of the impact of each factor on pod damage rate is $A>B>AC>B^2>AB>A^2>C$. The regression equation for the damage rate of the peanut-separating device is obtained:

$$Z_P =1.67 + 0.19A - 0.17B - 0.061C - 0.16AB - $$
$$0.17AC + 0.11A^2 + 0.16B^2 \qquad (20)$$

From Equation (20), it can be seen that the damage rate is linearly positively correlated with fan speed (A) and screen inclination angle (B) and linearly positively correlated with frequency (C). At the same time, it has a quadratic relationship with fan speed (A) and screen inclination angle (B). This indicates that an optimal combination of the three factors exists to minimize the damage rate of pods.
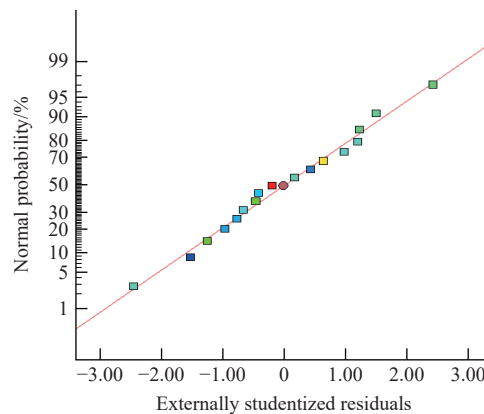
Figure 14   Damage ratio residuals normality plot

In terms of impurity rate analysis, as the wind speed of the fan increases, the impurity rate shows a decreasing trend. With the increase of the separating screen slope, the impurity rate shows a slow decreasing trend. With the increase in vibration frequency, the impurity rate shows a trend of initially decreasing and then increasing. Therefore, equipping the separating screen with a reasonable slope range and increasing the wind speed of the fan and vibration frequency can reduce the impurity rate of peanut pods, which promotes the performance of the separating screen.

In terms of damage rate analysis, as the wind speed of the fan increases, the damage rate shows an increasing trend. With the increase of the separating screen slope, the damage rate shows a slow decreasing trend. With the increase of vibration frequency, the damage rate shows a slow increasing trend. Therefore, equipping

the separating screen with a reasonable slope range and reducing wind speed and vibration frequency can reduce the damage rate of peanuts, which promotes the performance of the device.

3.3 Parameter optimization

From the variance analysis, it can be concluded that the factors affecting the peanut-separating operation are fan wind speed, screen tilt angle, and vibration frequency, and their significance may vary. Further optimization of parameters is required. Based on the operational requirements of the peanut-separating device, within a reasonable range of experimental factor levels, the optimization constraints are:

$$\begin{cases} \min Z_Z \\ \min Z_P \\ \text{s.t.} \begin{cases} 8 \leq X_1 \leq 10 \\ 5 \leq X_2 \leq 9 \\ 6 \leq X_3 \leq 8 \end{cases} \end{cases} \quad (21)$$

Based on the optimization module of Design Expert, the optimal parameter combination for the peanut- separating device operation is a fan wind speed of 8.9 m/s, screen tilt angle of 8.3°, and screen vibration frequency of 7.2 Hz. The corresponding impurity rate of the pods is 1.48%, and the damage rate is 1.61%. Continuation of validation tests is based on optimization results.

3.4 Validation test results

During field experiments, the separating device can operate continuously and normally. The impurity content and pod damage of the separating device are shown in Figures 15 and 16. The average impurity content of peanut pods in the separating device is 1.53%, with an error of 4% compared to the optimized results of the Box-Behnken central composite experiment. The average pod damage rate of peanut pods is 1.68%, with an error of 4.35% compared to the optimized results of the Box-Behnken central composite experiment. In the field verification test, the impurity content and damage rate of the peanut-separating device remain within a 5% error range compared to the optimized results of the experiment. It also meets and exceeds the technical index requirements for the design of the whole peanut combine harvester.
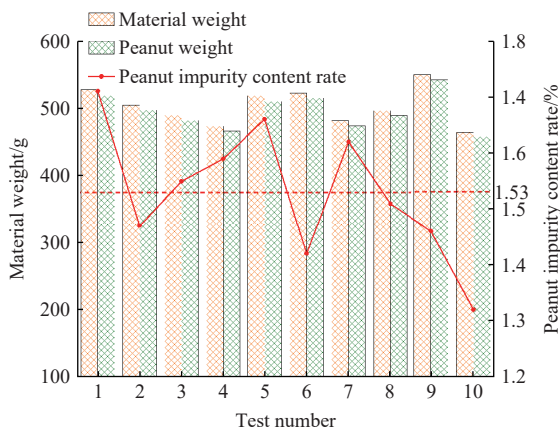
Figure 15   Field test results of peanut impurity content

In addition, it is important to verify further whether the optimal parameters of the device are reasonable in a number of comparative tests to take the average value. The test results are listed in Table 5.

During the forward movement of the machine, there was no material congestion. Moreover, the separation device was optimized for the separation effect at the best operating parameters. However, due to gaps in the sieve surface and side baffles, it is prone to

situations where vines get stuck. In the later stage, the installation position of the baffles can be adjusted to further improve the screening quality. In conclusion, this separating device has excellent screening performance and can effectively solve major challenges in the peanut harvesting process, such as high impurity rates and severe damage.
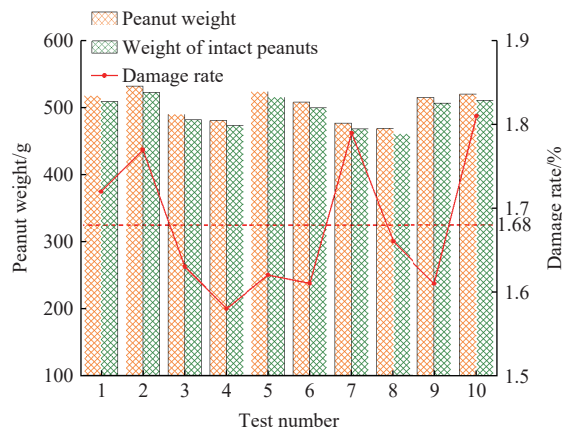
Figure 16   Field test results of peanut damage rate

Table 5   Comparison of test results

Test number	Fan wind speed X_1/(m·s^{-1})	Screen surface inclination X_2/(°)	Vibration frequency X_3/Hz	Impurity content ratio/%	Damage ratio/%
1	8	5	6	2.39%	1.96%
2	9	7	7	1.69%	1.81%
3	10	9	8	1.56%	1.78%
4	8.9	8.3	7.2	1.53%	1.68%

4   Conclusions

1) The separating device is a key piece of equipment for achieving high-quality peanut harvesting. By analyzing the working process of the peanut combine harvester, the motion coordination relationship of the separating device was determined.

2) A dynamic model of material sorting was constructed, and a wind selection simulation was conducted. The factors that affect the separating effect were determined as follows: wind speed of the fan, inclination angle of the screen, and frequency. Parameters were optimized through Box-Behnken central composite experiments, and the corresponding optimal values were obtained: fan wind speed of 8.9 m/s, inclination angle of the separating sieve surface with respect to horizontal at 8.3°, and vibration frequency of the separating sieve surface at 7.2 Hz. The corresponding impurity content of pods was 1.48%, and the separating damage rate was 1.61%.

3) The separating effect of the peanut harvester was verified through field experiments. The average impurity content of peanut pods after separating was 1.53%, the average impurity content error was 4%, the average damage rate of peanut pods was 1.68%, and the average damage rate error was 4.35%. These results meet the technical requirements for the overall design of the peanut combine harvester.

Acknowledgements

[References]

[1] Guan M. Research on full-feeding peanut picking test device and key components of peanut picker. PhD dissertation. Shengyang: Shengyang Agricultural University, 2017; 135p. (in Chinese)

[2] Zheng Y L. Experimental study on the air suction fresh peanut cleaning and removing device. Master dissertation. Shengyang: Shengyang Agricultural University, 2020; 67p. (in Chinese)

[3] Wang B, Hu Z C, Peng B L, Zhang Y H, Gu F W, Shi L L, et al. Structure operation parameter optimization for elastic steel pole oscillating screen of semi-feeding four rows peanut combine harvester. Transactions of the CSAE, 2017; 33(21): 20–28. (in Chinese).

[4] Gao L X, Chen Z Y, Charles C, Butts C L. Development course of peanut harvest mechanization technology of the United States and enlightenment to China. Transactions of the CSAE, 2017; 33(12): 1–9.

[5] Wang Y F. Design of the cleaning device for the peanut combine harvester and performance studies. Master dissertation. Qinhuangdao: Hebei Normal University of Science & Technology, 2022; 95p.(in Chinese)

[6] Wang D W, Shang S Q, Li X, Gao D X. Type L cleaning separation mechanism of peanut combine harvester. Transactions of the CSAM, 2013; 44(Supp.2): 68–74, 51. (in Chinese)

[7] Xu P Q, Dai F, Zhao W Y, Shi R J, Song X F, Qu J F. Simulation analysis and experiment of operation process of flax threshing and cleaning device. Transactions of the CSAM, 2023; 54(S1): 161–171. (in Chinese)

[8] Zhang D M. Study on working mechanism and experimental research of cleaning device for millet. PhD dissertation. Heilongjiang: Heilongjiang Bayi Agricultural University, 2023; 186p. (in Chinese)

[9] Kluge W. Neuzeitliche siebmaschinen fur die aufbereitung. Erdol and Kohle, 1975; 4: 705–711.

[10] Zhang N. Research on working mechanism and optimization analysis of chaffer sieve cleaning device in corn grain harvester. PhD dissertation. Changchun: Jilin University, 2023; 156p. (in Chinese)

[11] Dai F, Zhao W Y, Song X F, Shi R J, Liu G C, Wei B. Parameters optimization and experiment on separating and cleaning machine for flax threshing material. Transactions of the CSAM, 2020; 51(7): 100–108. (in Chinese)

[12] Wang S S, Lu M Q, Hu J P, Chen P, Ji J T, Wang F M. Design and experiment of Chinese cabbage seed threshing device combined with elastic short-rasp-bar tooth. Transactions of the CSAM, 2021; 52(11): 86–94. (in Chinese)

[13] Wan X Y, Yuan J C, Yang J, Liao Y T, Liao Q X. Effects of working parameters on the performance of cyclone separator for rapeseed combine harvester based on CFD. Int J Agric & Biol Eng, 2023; 16(1): 128–135.

[14] Tang H, Xu C S, Zhao J L, Wang Y J. Screening and impurity removal device to improve the accuracy of moisture content detection device for rice. Int J Agric & Biol Eng, 2022; 15(6): 113–123.

[15] Yang M, Zhang Y H, Zhang C, Gu F W, Yu Z Y, Hu Z C. Design and experiment of fan-sieve combined peanut film seedling separating device based on shredding and separating. Transactions of the CSAM, 2020; 51(12): 112–121. (in Chinese)

[16] Li X Y, Du Y F, Mao E R, Zhang Y, Liu L, Guo D F. Design and experiment of corn low damage threshing device based on DEM. Int J Agric & Biol Eng, 2023; 16(3): 55–63.

[17] Zhou L. Design and testing of a floor-standing jujube picking-conveyor cleaning device. Master dissertation. Shihezi: Shihezi University, 2020; 80p. (in Chinese)

[18] Li H C, Li Y M, Tang Z, Xu L Z, Zhao Z. Numerical simulation and analysis of vibration screening based on EDEM. Transactions of the CSAE, 2011; 27(5): 117–121. (in Chinese)

[19] Wu D L, Ding D, Cui B W, Jiang S, Zhao E L, Liu Y Y, et al. Design and experiment of vibration plate type camellia fruit picking machine. Int J Agric & Biol Eng, 2022; 15(4): 130–138.

[20] Feng Y L, Yin X C, Jin H R, Tong W Y, Ning X F. Design and experiment of a Chinese chive harvester. Int J Agric & Biol Eng, 2023; 16(2): 125–131.

[21] Du X, Jiang F, Li S, Xu N, Li D W, Wu C. Design and experiment of vibratory harvesting mechanism for Chinese hickory nuts based on orthogonal eccentric masses. Computers and Electronics in Agriculture, 2019; 156: 178–186.

[22] Wang B, Hu Z C, Wu N, Zhang Y H. Desing and experiments of 4HZB-2A peanut picker. Chinese Agricultural Mechanization, 2012; 1: 111–114. (in Chinese)

[23] Chen Z Y, Gao L X, Chen C, Butts C L. Analysis on technology status and development of peanut harvest mechanization of China and the United States. Transactions of the CSAM, 2017; 48 (04): 1–21. (in Chinese)

[24] Hou J L, Wang H X, Niu Z R, Tang R, Li T H. Discrete element simulation and experiment of picking and clearing performance of garlic seed-picking device. Transactions of the CSAE, 2019; 35(24): 48–57. (in Chinese)

[25] Zhang P, Xu H B, Hu Z C, Chen Y Q, Cao M Z, Yu Z Y, et al. Characteristics of agricultural dust emissions from harvesting operations: Case study of a whole-feed peanut combine. Agriculture, 2021; 11: 1068.

[26] Li D J, Shang S Q, He X N, Zhao Z, Chang Z C, Wang Y T, et al. Experiments and analysis of a peanut semi-feeding picking mechanism based on the JKR model. Agriculture, 2022; 12: 1418.

[27] Yan J C, Xie H X, Wei H, Wu H C, You Z Y. Optimizing the drying parameters of a fixed bed with reversing ventilation for peanut using computer simulation. Int J Agric & Biol Eng, 2021; 14(5): 255–266.

[28] Wang Z B, Wang Z W, Zhang Y P, Yan W X, Chi Y J, Liu C Q. Design and test of longitudinal axial flexible hammer-calw corn thresher. Transaction of CASM, 2020; 51(S2): 109–117. (in Chinese)